RSC Advances

ROYAL SOCIETY OF CHEMISTRY

www.rsc.org/advances

Tribological behavior of a TiAl matrix composite containing 10wt.%Ag investigated at four wear stages

Kang Yang [a], Xiaoliang Shi [a]*, Da Zheng [b], Wenzheng Zhai [a], Ahmed Mohamed Mahmoud Ibrahim [a], Zhihai Wang [a]

a. School of Mechanical and Electronic Engineering, Wuhan University of Technology, 122 Luoshi Road, Wuhan 430070, China

b. School of Mechanical Engineering, Shanghai Jiao Tong University, 1954 Huashan Road, Shanghai 200030, China

Abstract: The using longevity of mechanical components like gear and sliding bearing was related with their tribological behavior. The tribological behavior of TiAl matrix composite containing 10wt.%Ag (TiAl-10wt.%Ag) was investigated at the different four wear stages. Wear stages, which were identified by the obtained friction coefficient and wear rate, were divided into the initial wear stage (***INITIAL***), fast wear stage (***FAST***), stable wear stage (***STABLE***) and severe wear stage (***SEVERE***). The results showed that tribological behavior at ***INITIAL*** was improved for work hardening. Friction coefficient and wear rate at ***FAST*** were small for the forming of mixed layer containing solid lubricant Ag. Excellent tribological behavior at ***STABLE*** was attributed to the existence of lubricant film containing massive solid lubricant Ag. Poor tribological behavior of TiAl-10wt.%Ag at ***SEVERE*** was obtained for the lubricant film destroyed by the propagation of fatigue crack. It was found that

* **Corresponding author.** Tel./Fax: +86-27-87651793. E-mail address: sxl071932@126.com (X.L. Shi)

TiAl-10wt.%Ag, for the excellent tribological behavior at ***STABLE***, could be chosen as the promising structure material of mechanical components.

Keywords: Sliding wear; Solid lubricants; Electron microscopy; Surface analysis

1. Introduction

TiAl alloy, for its eminent mechanical behavior and thermal property, was accepted as the promising structure materials of aerospace components like turbine blades, divergent flap, turbocharger or nozzles, etc[1-5]. Mechanical components were fabricated using the materials of poor tribological performance, resulting in the wasting of materials and energy sources. TiAl alloy, for the poor tribological property, was also limited to further develop in the aerospace and automotive industries[6-9].

Tribological performance of material could be significantly improved by fabricating the self-lubricating composite containing solid lubricants. Solid lubricants such as MoS_2[10], multilayer graphene[11], graphite[12-15], boron nitride[16], Ti_3SiC_2[17, 18], multi-walled carbon nanotubes (MWCNTs)[19] and silver (Ag)[20] have been demonstrated to significantly improve the tribological property of self-lubricating composite. Shi et al.[20] fabricated TiAl matrix self-lubricating composite containing 10wt.%Ag (TiAl-10wt.%Ag) by adding solid lubricant Ag into TiAl alloy, and found the tribological performances of TiAl-10wt.%Ag were more excellent at the temperatures of 25-800°C, if compared to those of TiAl alloy, TiAl-5wt.%Ag and TiAl-15wt.%Ag.

After the three wear stages of fast wear, stable wear and severe wear[21], the failure of mechanical components was caused due to the excessive wear of materials. It was

generally thought that the period of stable wear was in more close relation with the using longevity of mechanical components, if compared to that of fast wear or severe wear. The period of stable wear could be significantly prolonged by shortening the periods of fast wear and severe wear, resulting in the improving of the using longevity of material. In order to explore the using longevity of mechanical components (gear and sliding bearing) of TiAl-10wt.%Ag, the tribological behavior of TiAl-10wt.%Ag would be respectively discussed at the different wear stages. To the best of our knowledge, it was rarely reported that the tribological test of 600min sliding was divided into the four wear stages according to the obtained friction coefficient and wear rate, and the tribological behavior of TiAl-10wt.%Ag was respectively discussed at the different four wear stages.

In this study, TiAl-10wt.%Ag was chosen as the material of sliding tribological tests for its excellent thermal property and mechanical performance. The friction coefficient and wear rate were continuously obtained during the 600min sliding wear. The four wear stages of TiAl-10wt.%Ag were judged by the acquired friction coefficient and wear rate. The tribological behaviors of TiAl-10wt.%Ag at the different four wear stages were respectively analyzed by studying the subsurface hardness of wear scar, wear mechanisms, the surface texture of wear scar and the cross-section micrographs of wear scar, as well as the distribution of solid lubricant Ag.

2. Experimental details

2.1 Materials

Spark plasma sintering (SPS) of D.R. Sinter® SPS3.20 apparatus (Sumitomo Coal & Mining, now SPS Syntex Inc.) was adopted to fabricate TiAl-10wt.%Ag (48at.%Ti-47at.%Al-2at.%Cr-2at.%Nb-1at.%B-10wt.%Ag). TiAl-10wt.%Ag consisted of Ti (20μm in average size (IAS), 99.9% in purity (IP)), Al (20μm IAS, 99.9% IP), B (25μm IAS, 99.9% IP), Nb (10μm IAS, 99.9% IP), Cr (10μm IAS, 99.9% IP) and Ag (74μm IAS, 99.95% IP). Before SPS process, the powders of Ti, Al, B, Nb, Cr and Ag were mixed using the vibration milling with the frequency of 45Hz. The mixed powders were loaded into the graphite molds of the inner diameter of 25mm, and sintered for 10min at the temperature and pressure of 1100ºC and 30MPa in pure Ar atmosphere protection. The heating rate of 100ºC/min was chosen in this study.

2.2 Vicker's microhardness and density

ASTM standard E92-82 was strictly executed to test Vicker's hardness of TiAl-10wt.%Ag using the Vicker's hardness apparatus of HVS-1000[22]. Ten tests were respectively executed to obtain the mean hardness of 5.97GPa. In accordance with the ASTM Standard B962-08[23], the Archimedes' principle was employed to attain the mean density of 4.22g/cm^3.

2.3 Tribological test

In order to explore the tribological behavior of TiAl-10wt.%Ag, the sliding tribological tests were repeatedly carried out on the high temperature tribometer of HT-1000 (made in Zhong Ke Kai Hua Corporation, China) on the basis of ASTM Standard G99-95[24]. At the sliding velocity and applied load of 0.5m/s and 12N, the

TiAl-10wt.%Ag of 25mm diameter rotated against the Si_3N_4 balls of 6mm diameter. Three tribological tests were tautologically executed for 600min to acquire the mean wear rate at 45-65% relative humidity. During the 600min sliding wear, the friction coefficient was automatically recorded by the computer system of HT-1000. The wear rates of TiAl-10wt.%Ag at the different sliding time were respectively calculated using the formula of wear rate, as shown in formula 1[25]:

$$W = \frac{V}{FL} \tag{1}$$

where V was wear volume, F was applied load and L was sliding distance. The wear volume V of TiAl-10wt.%Ag could be obtained by measuring the cross-section area A of wear scar using the surface profiler of ST400.

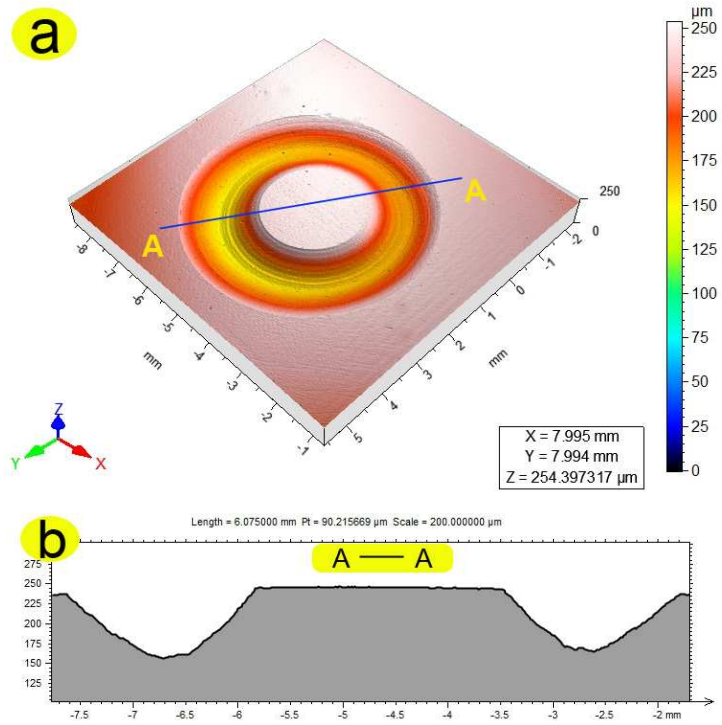

Fig.1 Representative morphologies of wear scar of TiAl-10wt.%Ag sliding against Si_3N_4 balls: 3D profile of wear scar (a), 2D profile of wear scar (b)

Fig.1 showed the representative morphologies of wear scar of TiAl-10wt.%Ag

sliding against Si_3N_4 balls. As shown in **Fig.1**, when the measured stylus of surface profilometer (ST400) slowly moved across wear scar along the straight line *AA* (see 3D profile of wear scar in **Fig.1a**), the coordinate positions of measured stylus were continuously recorded to form a 2D cross-section profile (see **Fig.1b**). Similarly, three tests were repeatedly executed to acquire the mean cross-section area *A* of wear scar. Wear volume *V* of wear scar could be calculated using the formula of wear volume *V* ($V=A\cdot L$), where *A* was the cross-section area of wear scar and *L* was the perimeter of wear scar[20].

2.4 Microstructure analysis

TiAl-10wt.%Ag was examined by the XRD with CuKα radiation at the scanning velocity of $0.01^{o}s^{-1}$. Cross-section area *A* of wear scar was measured by the surface profiler of ST400 (Nanovea). Morphologies of wear scar of TiAl-10wt.%Ag were analyzed by the electron probe microanalysis of JAX-8230 (EPMA). Cross-section micrographs of wear scars were analyzed by a SIRION 200 field emission scanning electron microscope (FESEM).

3. Results and discussion

3.1 Compositions of TiAl-10wt.%Ag

Fig.2 showed the typical XRD pattern of TiAl-10wt.%Ag fabricated by SPS. As was obvious in **Fig.2**, TiAl-10wt.%Ag was mainly composed of TiAl and Ag according to the intensity of different diffraction peaks.

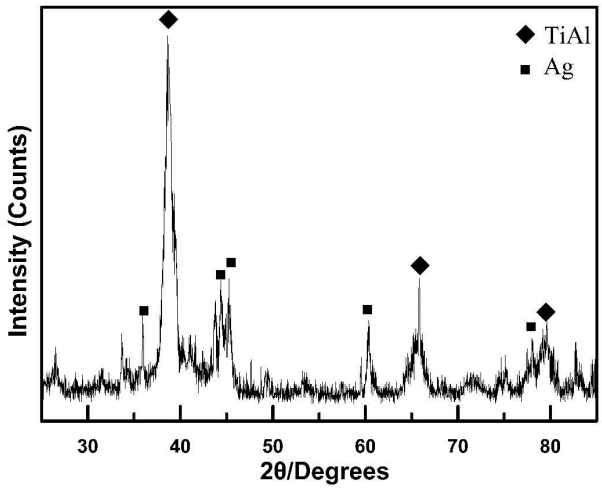

Fig.2 Typical XRD pattern of TiAl -10wt.%Ag fabricated by SPS

Fig.**3** exhibited the microstructure and elemental distribution of the cross-section of TiAl-10wt.%Ag. As shown in **Fig**.**3**, the solid lubricant Ag was uniformly distributed in TiAl-10wt.%Ag.

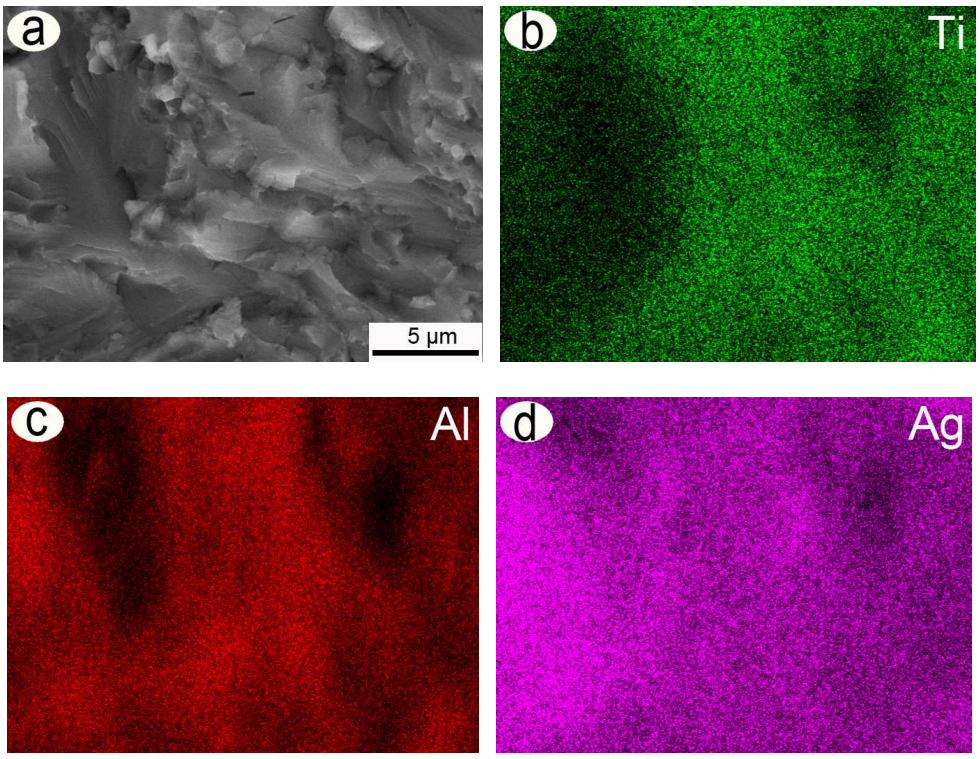

Fig.3 Microstructure and elemental distribution of the cross-section of TiAl-10wt.%Ag

3.2 Friction coefficient and wear rate

Fig.4 showed the representative friction coefficients of TiAl-10wt.%Ag at the different four wear stages. As was shown in **Fig.4a**, the smaller friction coefficients of TiAl-10wt.%Ag were obtained, if compared to those of TiAl alloy. According to the acquired friction coefficients, the tribological test of 600min sliding could be approximately divided into the initial wear stage (***INITIAL***) from 0 to 15min, fast wear stage (***FAST***) from 15 to 60min, stable wear stage (***STABLE***) from 60 to 585min and severe wear stage (***SEVERE***) from 585 to 600min.

INITIAL: As shown in **Fig.4a**, friction coefficients rapidly decreased with the increasing of sliding time in the range of 0-15min. Mean friction coefficient of 0.40 (see **Fig.4b**) and standard deviation (STDEV) of friction coefficients (0.11, see **Fig.4c**) were respectively obtained.

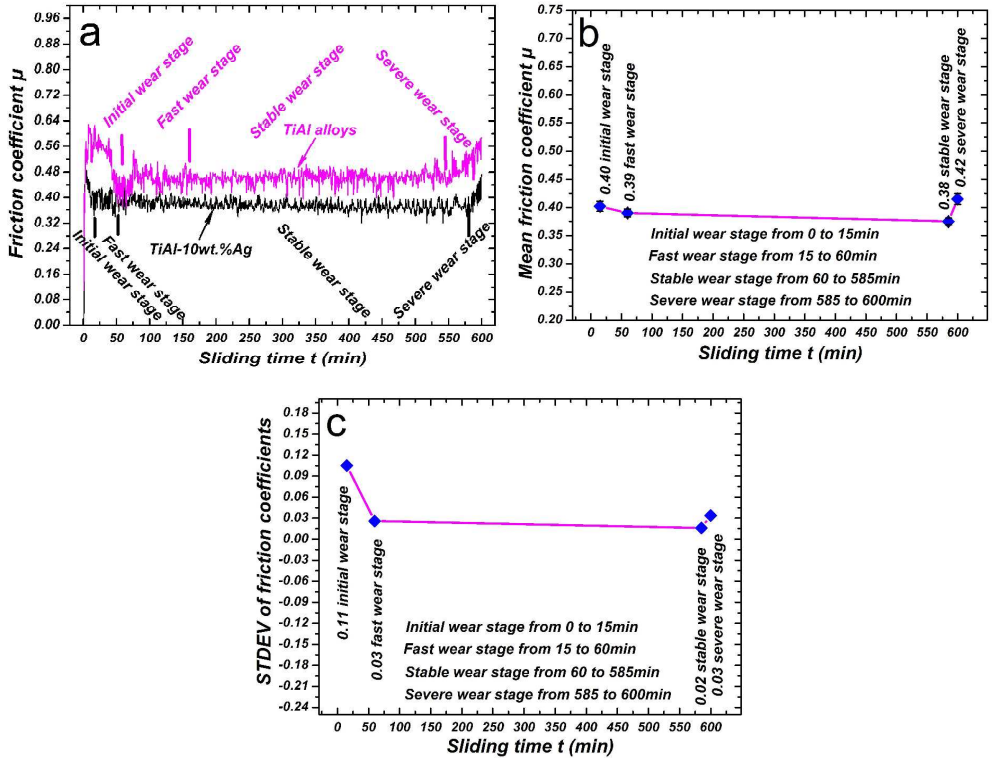

Fig.4 Representative friction coefficients of TiAl -10wt.%Ag at the different four friction stages: dynamic friction coefficients (a), mean friction coefficients (b) and STDEV of friction coefficients (c)

FAST: In **Fig.4a**, friction coefficients gradually decreased with an increase in sliding time of 15-60min. Mean friction coefficient and STDEV of friction coefficients were 0.39 (see **Fig.4b**) and 0.03 (see **Fig.4c**).

STABLE: Friction coefficients (see **Fig.4a**) slightly fluctuated with the increasing of sliding time from 60 to 585min. Mean friction coefficient (0.38, see **Fig.4b**) and STDEV of friction coefficients (0.02, see **Fig.4c**) were severally obtained.

SEVERE: As was clear in **Fig.4a**, friction coefficients showed the upward trend, when sliding time increased from 585min up to 600min. The mean friction coefficient of 0.42 (see **Fig.4b**) and STDEV of 0.03 (see **Fig.4c**) were severally attained.

Mean friction coefficients and STDEV of friction coefficients continually decreased with the increasing of sliding time of 0-585min (***INITIAL*** from 0 to 15min, ***FAST*** from 15 to 60min and ***STABLE*** from 60 to 585min), and then increased with the increasing of sliding time in the range of 585-600min (***SEVERE*** from 585 to 600min). The period of stable wear (from 60 to 585min) was prolonged up to 525min for the existence of solid lubricant Ag, if compared to 390min (from 160 to 550min) of TiAl alloy. The smaller mean friction coefficient (0.38) and the lower STDEV (0.02) of friction coefficients were severally obtained at ***STABLE***, if compared to those at ***INITIAL***, ***FAST*** and ***SEVERE***.

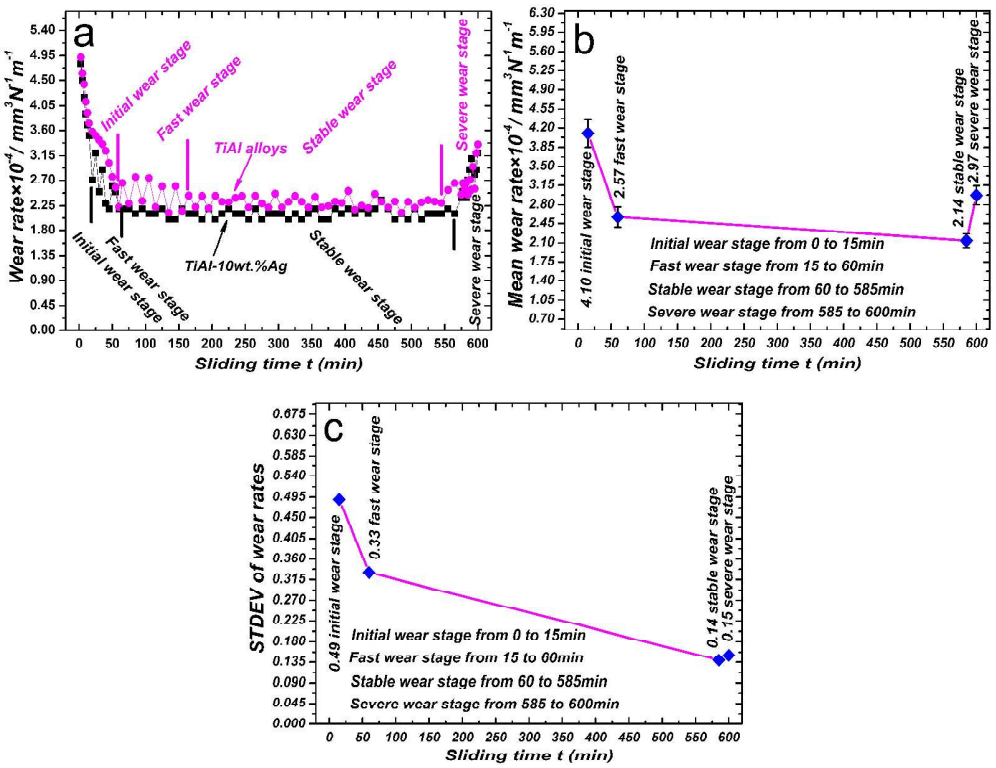

Fig.5 Typical wear rates of TiAl-10wt.%Ag at the different four friction stages: dynamic wear rates (a), mean wear rates (b) and STDEV of wear rates (c)

Fig.5 showed the typical wear rates of TiAl-10wt.%Ag at the different four wear stages. As shown in **Fig.5a**, the smaller wear rates of TiAl-10wt.%Ag were attained, if compared to those of TiAl alloy. In terms of the acquired wear rates, the tribological test of 600min sliding was also divided into ***INITIAL*** from 0 to 15min, ***FAST*** from 15 to 60min, ***STABLE*** from 60 to 585min and ***SEVERE*** from 585 to 600min.

INITIAL: As shown in **Fig.5a**, wear rates showed the rapidly downward trend with the increasing of sliding time from 0 to 15min. Mean wear rate ($4.10\times10^{4}mm^{3}N^{-1}m^{-1}$, see **Fig.5b**) and STDEV of wear rates (0.49, see **Fig.5c**) were respectively obtained.

FAST: In **Fig.5a**, wear rates showed the gradually downward trend with the increasing of sliding time of 15-60min. Mean wear rate and STDEV of wear rates

were $2.57\times10^{4}mm^{3}N^{-1}m^{-1}$ (see **Fig.5b**) and 0.33 (see **Fig.5c**).

STABLE: As was shown in **Fig.5a**, wear rates (see **Fig.5a**) showed the slight fluctuation with an increase in sliding time of 60-585min. Mean wear rate of $2.14\times10^{4}mm^{3}N^{-1}m^{-1}$ (see **Fig.5b**) and wear rate STDEV of 0.14 (see **Fig.5c**) were severally attained.

SEVERE: As was clear in **Fig.5a**, wear rates rapidly increased with the increasing of sliding time in the range of 585-600min. Mean wear rate of $2.97\times10^{4}mm^{3}N^{-1}m^{-1}$ (see **Fig.5b**) and STDEV of wear rates (0.15, see **Fig.5c**) were obtained.

Mean wear rate and STDEV of wear rates gradually decreased with the increasing of sliding time of 0-585min (***INITIAL*** from 0 to 15min, ***FAST*** from 15 to 60min and ***STABLE*** from 60 to 585min), and then increased with the increasing of sliding time in the range of 585-600min (***SEVERE*** from 585 to 600min). The smaller mean wear rate of $2.14\times10^{4}mm^{3}N^{-1}m^{-1}$ and the lower STDEV (0.14) of wear rates were severally obtained at ***STABLE***.

At ***STABLE***, the excellent tribological behavior of TiAl-10wt.%Ag was obtained due to the smaller friction coefficient, wear rate and STDEV. The period of stable wear (from 60min to 585min) was significantly prolonged up to 525min for the existence of solid lubricant Ag, if compared to 390min (from 160 to 550min) of TiAl alloy.

The wear resistance of material was in proportion to its hardness[26]. Subsurface hardness of wear scar could be continually altered with the evolving of subsurface microstructure[27]. Hence, it was significant to study effect of subsurface hardness on

the tribological performance of TiAl-10wt.%Ag.

3.3 Influence of subsurface hardness of wear scar on tribological behavior of TiAl-10wt.%Ag

Fig.6 showed the representative subsurface hardness of wear scar of TiAl-10wt.%Ag at the different four wear stages. As shown in **Fig.6**, subsurface hardness of wear scar was respectively studied at the four stages of ***INITIAL*** from 0 to 15min, ***FAST*** from 15 to 60min, ***STABLE*** from 60 to 585min and ***SEVERE*** from 60 to 585min.

INITIAL: As shown in **Fig.6a**, when sliding time increased up to 15min, the subsurface hardness of wear scar was continuously improved for work hardening, resulting in the improving of the tribological behavior of TiAl-10wt.%Ag. Mean subsurface hardness of 6.16GPa (see **Fig.6b**) and STDEV of subsurface hardness (0.12, see **Fig.6c**) were respectively acquired.

FAST: In **Fig.6a**, subsurface hardness of wear scar was further improved with the increasing of sliding time in the range of 15-60min, leading to the further decreasing of mean friction coefficient and wear rate. Mean subsurface hardness and STDEV of subsurface hardness of wear scar were 6.14GPa (see **Fig.6b**) and 0.13 (see **Fig.6c**) respectively.

STABLE: As was shown in **Fig.6a**, small subsurface hardness of wear scar showed the slight fluctuation with the increasing of sliding time of 60-585min, resulting in the acquiring of the excellent tribological behavior of TiAl-10wt.%Ag. Mean subsurface hardness (6.07GPa, see **Fig.6b**) and STDEV of subsurface hardness (0.09, see **Fig.6c**)

were severally obtained.

SEVERE: As was clear in **Fig.6a**, the high subsurface hardness of wear scar was rapidly improved with an increase in sliding time of 585-600min, leading to the lowering of the tribological behavior of TiAl-10wt.%Ag. The mean subsurface hardness of 6.20GPa (see **Fig.6b**) and STDEV of subsurface hardness (0.14, see **Fig.6c**) were severally obtained.

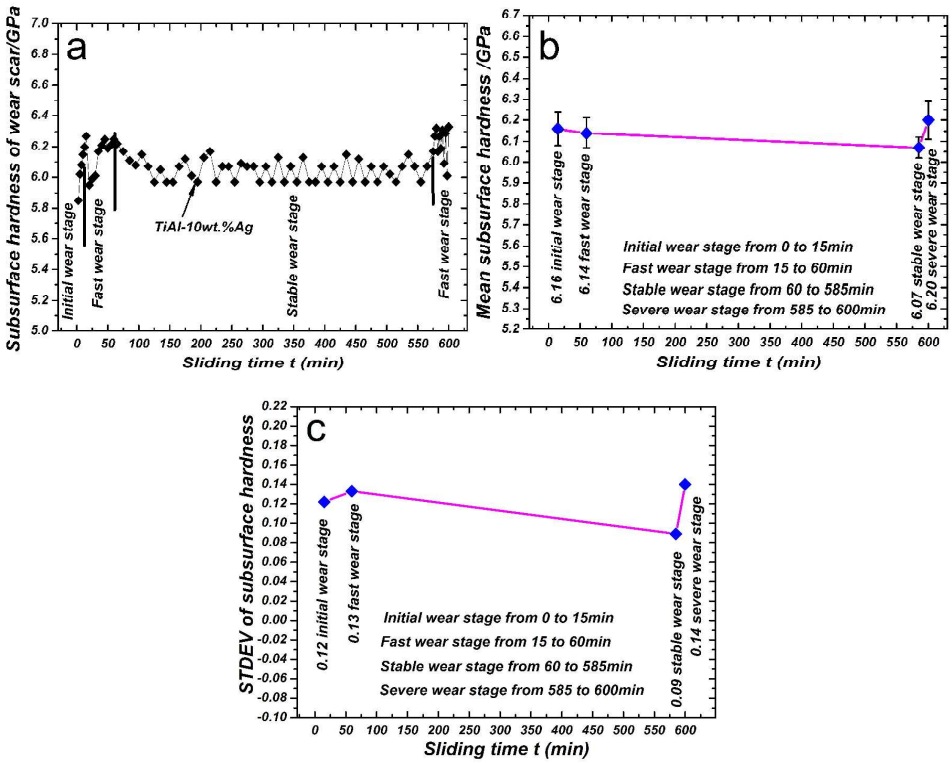

Fig.6 Representative subsurface hardness of wear scar of TiAl-10wt.%Ag at the different four friction stages: dynamic subsurface hardness (a), mean subsurface hardness (b) and STDEV of subsurface hardness (c)

Mean subsurface hardness and STDEV of subsurface hardness was gradually lowered with the increasing of sliding time in the range of 0-585min (***INITIAL*** from 0 to 15min, ***FAST*** from 15 to 60min and ***STABLE*** from 60 to 585min), and then was

significantly improved with the increasing of sliding time of 585-600min (***SEVERE*** from 585 to 600min). The small mean subsurface hardness of 6.07GPa and the smaller STDEV (0.09) of subsurface hardness were respectively obtained at ***STABLE***.

When the subsurface hardness of wear scar was continually improved for work hardening during the 15min sliding wear, the friction coefficient and wear rate of TiAl-10wt.%Ag at ***INITIAL*** showed the gradually downward tendency. When sliding time increased from 15 to 60min, the subsurface hardness of wear scar at ***FAST*** exhibited the gradually upward trend, leading to the further improving of the tribological behavior of TiAl-10wt.%Ag. When sliding time increased from 60min up to 585min, the subsurface hardness of wear scar showed the slight fluctuation for the smaller STDEV (0.09) of subsurface hardness, resulting in the acquiring of small friction coefficient and wear rate at ***STABLE***. The subsurface hardness of wear scar was rapidly improved with the increasing of sliding time of 585-600min, and the tribological behavior of TiAl-10wt.%Ag at ***SEVERE*** was significantly lowered. The more excellent tribological behavior of TiAl-10wt.%Ag was obtained at ***STABLE***, if compared to those at ***INITIAL***, ***FAST*** and ***SEVERE***. Evan et al.[26] thought that the lower subsurface hardness of wear scar was corresponding to the high friction coefficient and wear rate. The view of Evan was consistent with our research results at ***INITIAL*** and ***FAST***, but was inconsistent with our research conclusions at ***STABLE*** and ***SEVERE***. Hence, in order to obtain the reasonable explanation, the tribological behavior of TiAl-10wt.%Ag would be further investigated by analyzing the morphology of wear scar, the surface texture of wear scar, the cross-section

morphologies of wear scar and the distribution of solid lubricant Ag.

3.4 Effect of wear mechanism and surface texture on tribological behavior of TiAl-10wt.%Ag

Wear mechanisms at the four wear stages could be judged by the morphologies of wear scar of TiAl-10wt.%Ag. The morphology of wear scar was examined by the surface texture of the height parameters. The height parameters used in this study mainly contained the arithmetical mean height of surface (Sa), the root mean square height (Sq) and the kurtosis of height distribution (Sku). Mean roughness of wear scar was measured by the Sa. Standard deviation of height distribution of wear scar could be evaluated using the Sq. Flatness of wear scar was measured by the Sku.

Fig.7 showed the typical electron probe morphology and surface texture of wear scar of TiAl-10wt.%Ag at ***INITIAL***. As shown in **Fig.7a**, massive peeling pits and big grooves existed on wear scar. It was apparent that the primary wear mechanisms were peeling and plough at ***INITIAL***. In **Fig.7b**, the poor surface texture of wear scar was obtained for the high Sa (0.518), Sq (0.478) and Sku (8.166).

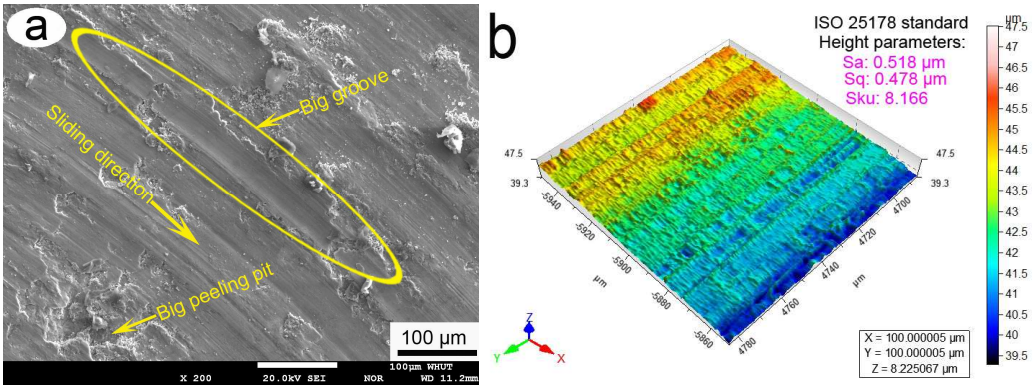

Fig.7 Typical electron probe morphology and surface texture of wear scar of TiAl-10wt.%Ag at ***INITIAL***: morphologies of wear scar (a) and surface texture of

wear scar (b)

Fig.8 showed the representative electron probe morphology and surface texture of wear scar of TiAl-10wt.%Ag at ***FAST***. Massive abrasive debris and continuous grooves were on wear scar at ***FAST***. It was obvious that the dominant wear mechanism was abrasive wear. The surface texture of Sa (0.478), Sq (0.438) and Sku (7.666) was improved at ***FAST***, if compared to that at ***INITIAL***.

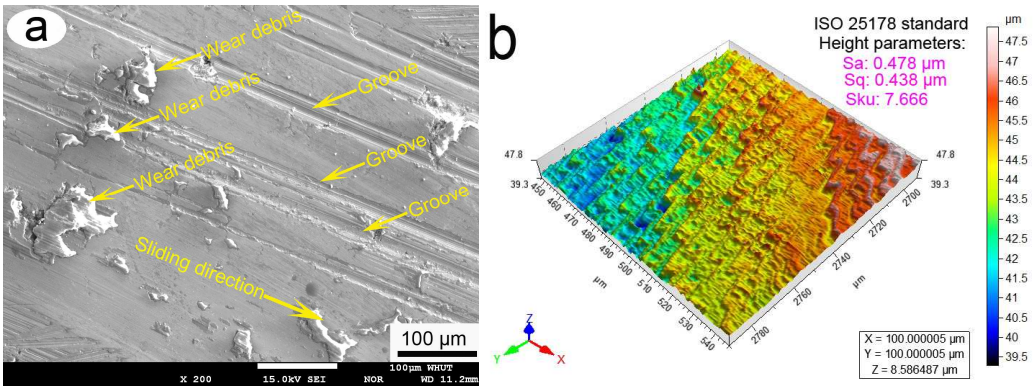

Fig.8 Representative electron probe morphology and surface texture of wear scar of TiAl-10wt.%Ag at ***FAST***: morphologies of wear scar (a) and surface texture of wear scar (b)

Fig.9 showed the typical electron probe morphology and surface texture of wear scar of TiAl-10wt.%Ag at ***STABLE***. Small and flat wear debris, shallow grooves existed on the smooth wear scar. It was evident that the main wear mechanism was plastic deformation at ***STABLE***. The more excellent surface texture was obtained for the smaller Sa (0.398), Sq (0.359) and Sku (6.866) at ***STABLE***.

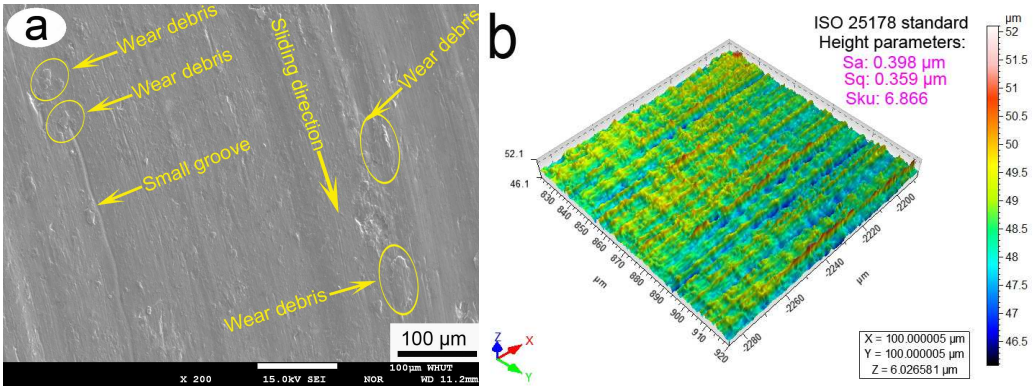

Fig.9 Typical electron probe morphology and surface texture of wear scar of TiAl-10wt.%Ag at ***STABLE***: morphologies of wear scar (a) and surface texture of wear scar (b)

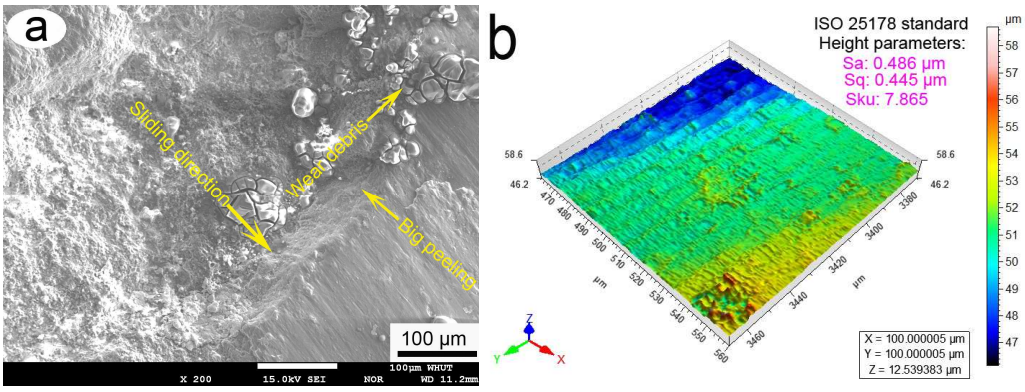

Fig.10 Typical electron probe morphology and surface texture of wear scar of TiAl-10wt.%Ag at ***SEVERE***: morphologies of wear scar (a) and surface texture of wear scar (b)

Fig.10 showed the typical electron probe morphology and surface texture of wear scar of TiAl-10wt.%Ag at ***SEVERE***. Big peeling and massive wear debris appeared on wear scar. It was obvious that the primary wear mechanisms were severe peeling and abrasive wear at ***SEVERE***. The poor surface texture of Sa (0.486), Sq (0.445) and Sku (7.865) was caused for the severe peeling at ***SEVERE***.

At ***STABLE***, the wear mechanism of plastic deformation was obtained. The

morphology of wear scar was significantly improved for the plastic deformation of soft metal Ag during the sliding process, resulting in the improving of surface texture of wear scar (Sa (0.398), Sq (0.359) and Sku (6.866)), the decreasing of frictional resistance, and the improving of tribological behavior of TiAl-10wt.%Ag. Hence, the excellent tribological behavior of TiAl-10wt.%Ag was acquired at ***STABLE***. To further explore the tribological behavior of TiAl-10wt.%Ag, the cross-section of wear scar needed to be respectively investigated at the different four wear stages.

3.5 Effect of cross-section of wear scar on tribological behavior of TiAl-10wt.%Ag

Fig.11 showed the representative FESEM micrographs of cross-sections of wear scars of TiAl-10wt.%Ag at the different four wear stages. **Fig.12** exhibited the typical XRD patterns of wear debris obtained at the different four wear stages. At the different four wear stages, the effect of the cross-section morphologies of wear scars on the tribological behavior of TiAl-10wt.%Ag were respectively analyzed.

INITIAL: As shown in **Fig.11a**, the significant morphologies of two layers were identified, which were marked as A and B. Layer A was known as the compacted layer of submicron grains for work hardening, resulting in the improving of subsurface hardness, and the lowering of friction coefficient and wear rate. Layer B consisting of large grains was named as the matrix material of TiAl-10wt.%Ag. As was clear in **Fig.12a**, wear debris at ***INITIAL*** primarily consisted of TiAl, Ag and Al_2O_3 according to the diffraction peak intensity of different phases. The presence of these phases indicated that during the sliding wear, the compacted layer (see layer A

in **Fig.11a**) containing TiAl, Ag and Al_2O_3 was gradually formed for the accumulation of wear debris.

FAST: As shown in **Fig.11b**, the significant morphologies of three layers were clearly identified. The three layers, which were marked as C, D and E, were called as the mixed layer, granular layer and TiAl matrix material, respectively. **Table 1** showed the elemental compositions (wt.%) of tested regions marked by 1-6 in **Fig.11b**. As was clear in **Table 1**, during the sliding process, soft metal Ag showed the upward migration for its plastic deformation, leading to the forming of mixed layer (layer C) containing massive Ag. Smaller friction coefficient and wear rate, for the mixed layer containing massive solid lubricant Ag, were acquired at ***FAST***, if compared to those at ***INITIAL***. As shown in **Fig.12b**, the diffraction peak of Ag phase further indicated that the mixed layer contained massive solid lubricant Ag.

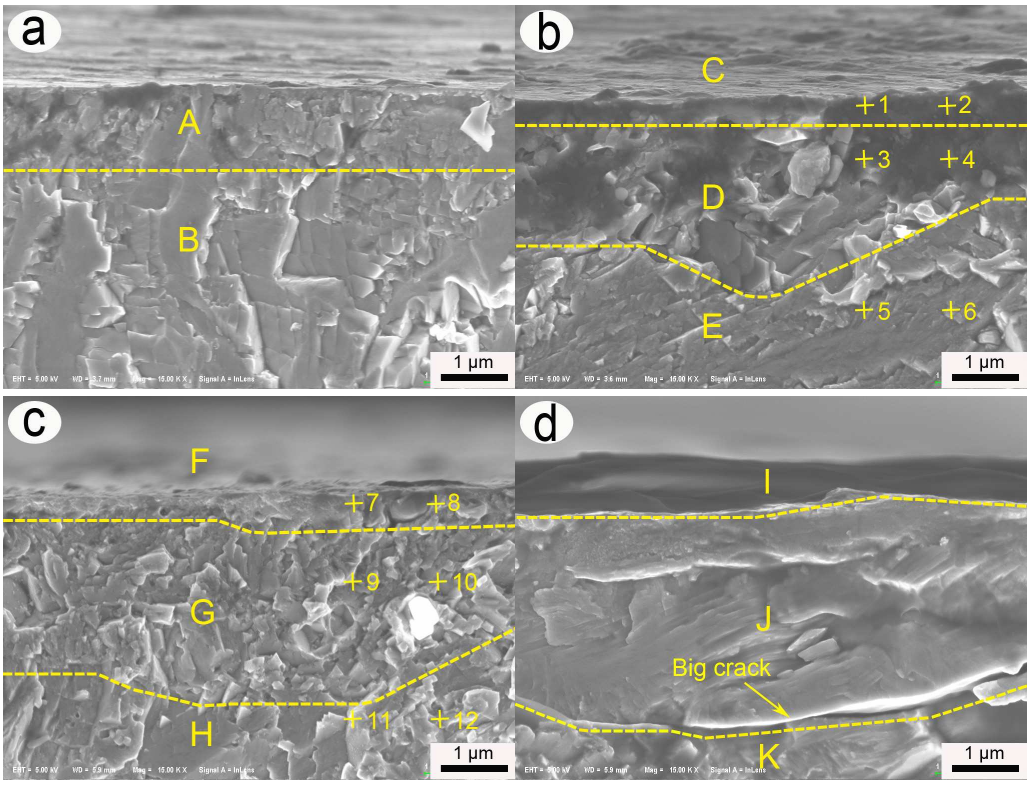

Fig.11 Representative FESEM micrographs of cross-sections of wear scars of TiAl-10wt.%Ag at the different four wear stages: ***INITIAL*** (a), ***FAST*** (b), ***STABLE*** (c) and ***SEVERE*** (d)

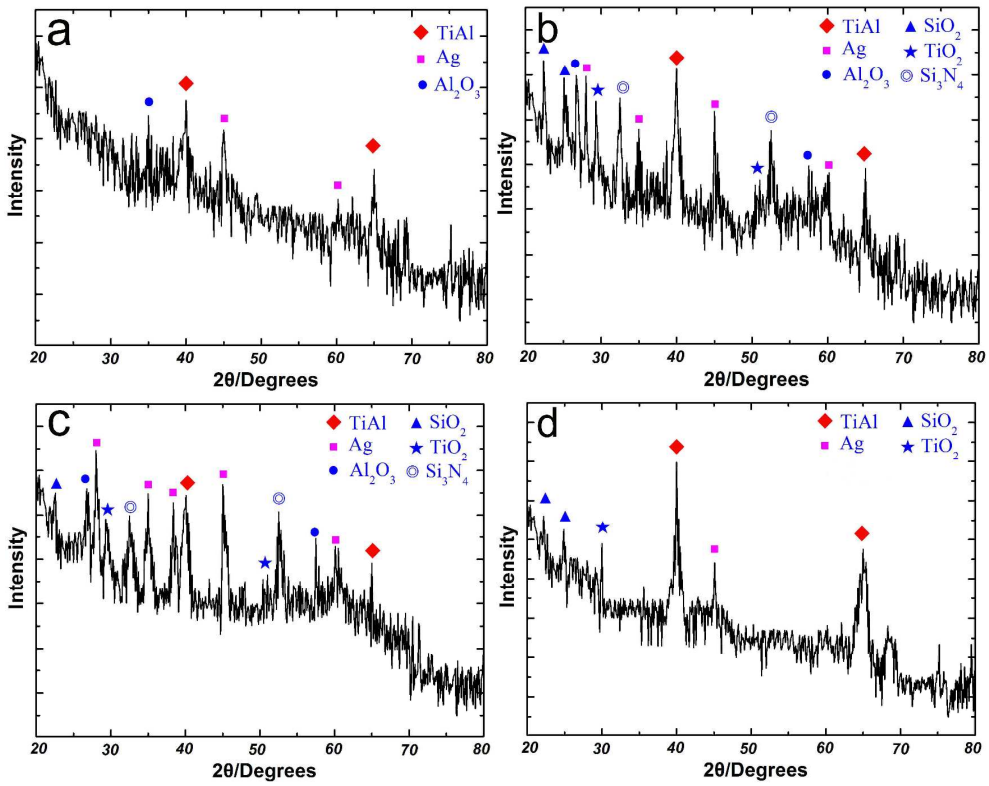

Fig.12 Typical XRD patterns of wear debris obtained at the different four wear stages: ***INITIAL*** (a), ***FAST*** (b), ***STABLE*** (c) and ***SEVERE*** (d)

Table 1 Elemental compositions (wt.%) of tested regions marked by 1-6 in **Fig.11b**

Element	1	2	3	4	5	6
Ti	31.24	33.67	36.76	37.66	45.97	48.89
Al	22.75	20.53	27.62	25.31	38.42	37.61
Ag	46.01	45.80	35.62	37.03	15.61	13.50

Table 2 Elemental compositions (wt.%) of tested regions marked by 7-12 in **Fig.11c**

Element	7	8	9	10	11	12

Ti	14.13	16.23	43.87	42.37	47.38	46.36
Al	11.66	13.75	34.40	37.41	42.51	45.41
Ag	74.21	70.02	21.73	20.22	10.11	8.23

STABLE: As was shown in **Fig.11c**, the three layers of F, G and H were known as the lubricant film, compacted layer and TiAl matrix material, respectively. **Table 2** showed the elemental compositions (wt.%) of tested regions marked by 7-12 in **Fig.11c**. The lubricant film (see layer F in **Fig.11c**) was rich in solid lubricant Ag, which existed above compacted layer (see layer G in **Fig.11c**), resulting in the improving of the tribological behavior of TiAl-10wt.%Ag, the acquiring of excellent surface texture (Sa (0.398), Sq (0.359) and Sku (6.866)). As was obvious in **Fig.12c**, lubricant film was mainly composed of TiAl, Ag, Al_2O_3, SiO_2, TiO_2 and Si_3N_4 according to the diffraction peak intensity of their phases. Hence, the lubricant film containing massive soft metal Ag existed above compacted layer at ***STABLE***, leading to the lowering of subsurface hardness of wear scar, and the improving of tribological behavior of TiAl-10wt.%Ag. The view[26], where the excellent tribological behavior was obtained for its high hardness, was given the reasonable explanation.

SEVERE: In **Fig.11d**, layer I, layer J and layer K were named as the lubricant film, compacted layer and TiAl matrix material, respectively. The lubricant film and compacted layer were severely destroyed for the propagation of fatigue crack, resulting in the improving of subsurface hardness, the forming of poor surface texture (Sa (0.486), Sq (0.445) and Sku (7.865)), the increasing of frictional resistance, and the improving of friction coefficient of TiAl-10wt.%Ag. The big peeling was caused

for the propagation of fatigue crack, and was removed from wear scar at the effect of inertia force, leading to the improving of wear rate of TiAl-10wt.%Ag. As shown in **Fig.12d**, wear debris at ***SEVERE*** mainly consisted of TiAl, Ag, SiO_2 and TiO_2 according to their diffraction peak intensity. The weak intensity of the diffraction peak of Ag phase further indicated that the lubricant film was destroyed at ***SEVERE***. The view of Evan[26], where the friction coefficient and wear rate decreased with the increasing of subsurface hardness, was also given the reasonable explanation.

At ***STABLE***, the lubricant film containing massive solid lubricant Ag (see **Table 2** and **Fig.11c**) was beneficial to the improvement of tribological performance and the lowering of subsurface hardness. The smooth morphology of wear scar was formed for the plastic deformation of soft metal Ag. The excellent surface texture of wear scar was obtained for the smaller Sa (0.398), Sq (0.359) and Sku (6.866). In order to further studied the effect of the lubricant film containing massive Ag on tribological performance, the distribution of solid lubricant Ag at ***STABLE*** needed to be studied.

3.6 Effect of distribution of solid lubricant Ag on tribological behavior of TiAl-10wt.%Ag

Fig.13 showed the microstructure and elemental distributions of wear scar of TiAl-10wt.%Ag at ***STABLE***. As shown in **Fig.13**, massive solid lubricant Ag was uniformly distributed on wear scar to form the lubricant film at ***STABLE***. The smooth morphology of wear scar was formed for the plastic deformation of Ag during the sliding wear.

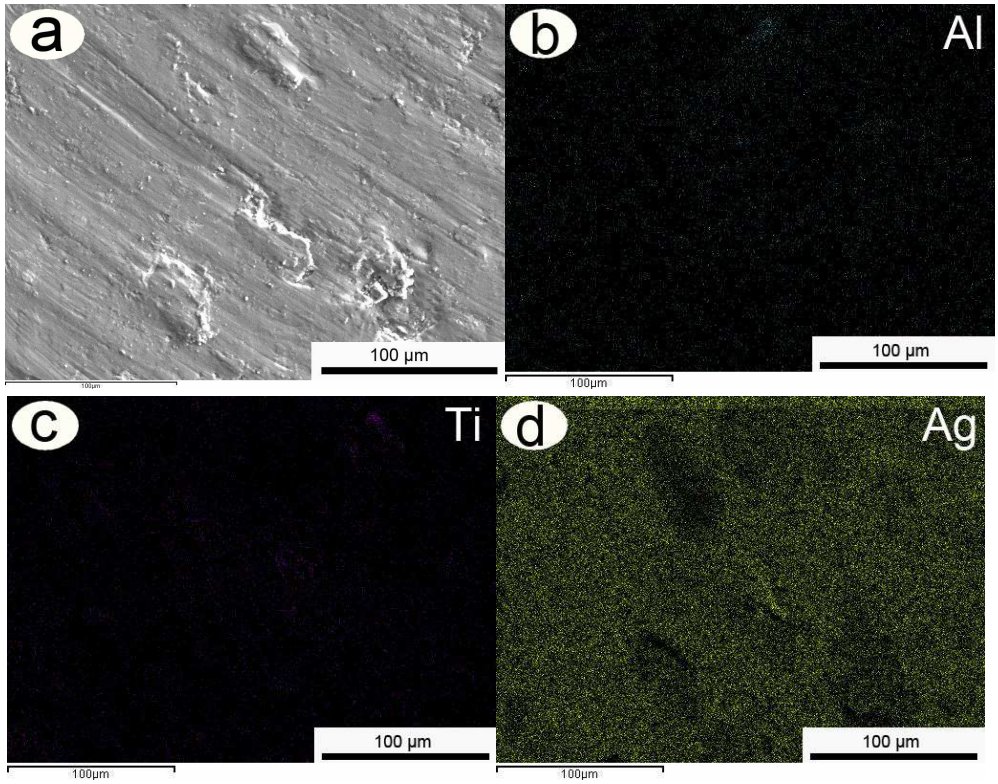

Fig.13 Microstructure and elemental distributions of wear scar of TiAl-10wt.%Ag at ***STABLE***

3.7 Mechanism analysis of TiAl-10wt.%Ag at the different four wear stages

In order to better analyze the tribological behavior of TiAl-10wt.%Ag, the wear mechanisms needed to be analyzed at the wear stages of ***INITIAL***, ***FAST***, ***STABLE*** and ***SEVERE***.

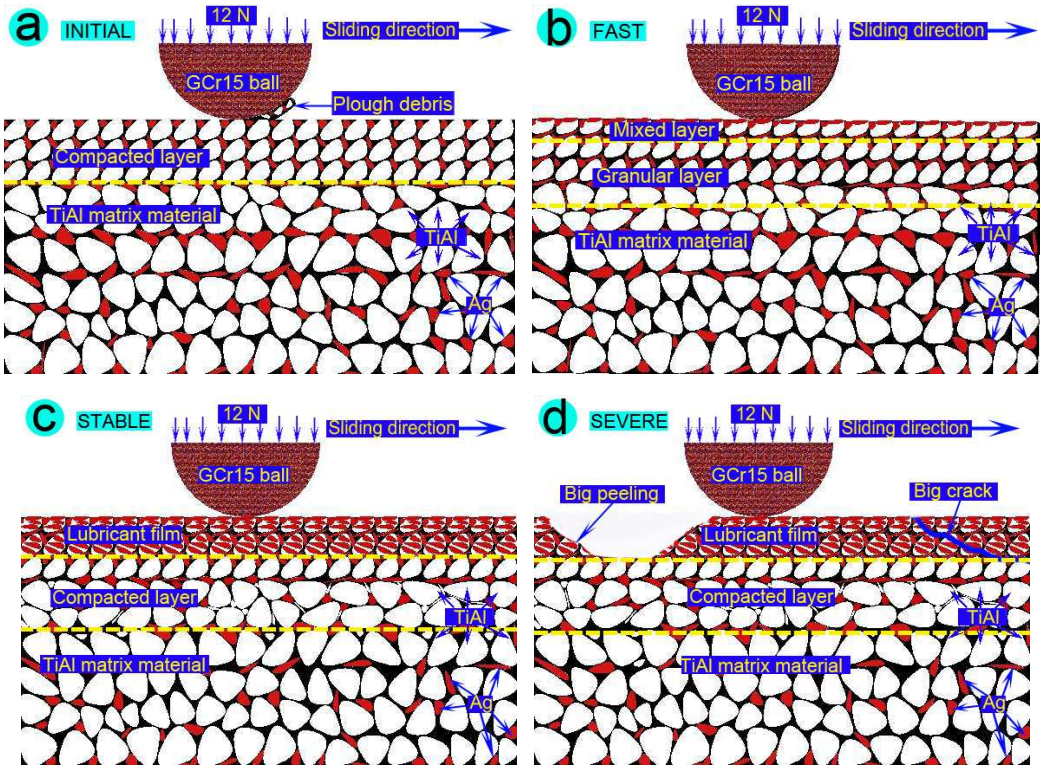

Fig.14 Schematic diagrams of the cross-section microstructures of wear scars of TiAl-10wt.%Ag at the different four wear stages: ***INITIAL*** (a), ***FAST*** (b), ***STABLE*** (c) and ***SEVERE*** (d)

Fig.14 showed the schematic diagrams of the cross-section microstructures of wear scars of TiAl-10wt.%Ag at the different four wear stages. As shown in **Fig.14a**, the big plough debris appeared on the wear scar of TiAl-10wt.%Ag under the condition of the wear mechanisms of peeling and plough at ***INITIAL***. At the repeating effect of the high pressure stress, the compacted layer was gradually formed for work hardening, resulting in the gradual improving of subsurface hardness, and the slow lowering of friction coefficient and wear rate. As was clear in **Fig.14b**, the big plough debris was refined into the small and hard wear debris at ***FAST***. Due to the repeating effect of the high pressure stress, the downward trend of small wear debris and the upward

tendency of solid lubricant Ag were obtained for the plastic deformation of Ag, resulting in the forming of mixed layer, the acquiring of the wear mechanism of abrasive wear, and the improving of subsurface hardness of wear scar. Hence, the tribological behavior of TiAl-10wt.%Ag was improved for the existence of the mixed layer containing massive Ag, if compared to that at ***INITIAL***. As was shown in **Fig.14c**, during the sliding process, the solid lubricant Ag was uniformly spread out on wear scar to form the lubricant film of antifriction and antiwear behavior. The small wear debris was continuously compacted to form the compacted layer at the effect of the high pressure stress. Hence, the main wear mechanism was plastic deformation, and the smaller friction coefficient and wear rate were obtained at ***STABLE***. The subsurface hardness of wear scar was lowered for the existence of lubricant film containing massive soft metal Ag. In **Fig.14d**, the big peeling appeared on wear scar for the propagation of fatigue crack, and was removed from the wear scar of TiAl-10wt.%Ag at the effect of inertia force, leading to the improving of subsurface hardness of wear scar, the improving of friction coefficient and wear rate, and the lowering of the stability of tribological tests.

In this study, the sliding tribological behavior of TiAl-10wt.%Ag was investigated. In accordance with the obtained friction coefficient and wear rate, the tribological test of 600min sliding was divided into the four wear stages of ***INITIAL*** from 0 to 15min, ***FAST*** from 15 to 60min, ***STABLE*** from 60 to 585min and ***SEVERE*** from 585 to 600min. The tribological behavior of TiAl-10wt.%Ag and the period of stable wear were significantly improved, if compared to those of TiAl alloy. At ***INITIAL***, the

wear mechanisms of peeling and plough were obtained. The subsurface hardness of wear scar of TiAl-10wt.%Ag was gradually improved for work hardening during the 15min sliding wear, resulting in the gradual forming of compacted layer, and the slow lowering of friction coefficient and wear rate. At ***FAST***, the wear mechanism of abrasive wear was acquired. During the sliding tribological test of 15-60min, the hard wear debris showed the downward motion tendency, and the solid lubricant Ag exhibited the upward migration trend for the plastic deformation of soft metal Ag, resulting in the forming of mixed layer, the improving of subsurface hardness of wear scar, and the improving of tribological behavior of TiAl-10wt.%Ag. At ***STABLE***, under the condition of the wear mechanism of plastic deformation, the solid lubricant Ag was uniformly spread out on wear scar to form lubricant film, and the excellent surface texture of Sa (0.398), Sq (0.359) and Sku (6.866) was obtained, leading to the improving of the contact area between TiAl-10wt.%Ag and Si_3N_4 balls, the lowering of subsurface hardness of wear scar, the decreasing of friction coefficient and wear rate, as well as the improving of tribological test stability. At ***SEVERE***, the severe peeling was caused for the propagation of fatigue crack during the sliding wear of 585-600min, and the poor surface texture of Sa (0.486), Sq (0.445) and Sku (7.865) was obtained, resulting in the lowering of the contact area between TiAl-10wt.%Ag and Si_3N_4 balls, the destroying of lubricant film, the improving of subsurface hardness of wear scar, the improving of friction coefficient and wear rate. Hence, the poor tribological behavior of TiAl-10wt.%Ag was caused for the propagation of fatigue crack. The friction coefficient and wear rate slowly decreased, and the STDEV of

friction coefficient and wear rate gradually lowered with the increasing of sliding time of 0-585min (***INITIAL*** from 0 to 15min, ***FAST*** from 15 to 60min and ***STABLE*** from 60 to 585min). The friction coefficient and wear rate, as well as the STDEV of friction coefficient and wear rate were rapidly improved with the increasing of sliding time of 585-600min (***SEVERE*** from 585 to 600min). Hence, the excellent tribological behavior was obtained for the existence of lubricant film at ***STABLE***.

4. Conclusions

In this study, the tribological behavior of TiAl-10wt.%Ag was respectively studied at the four wear stages of ***INITIAL*** from 0 to 15min, ***FAST*** from 15 to 60min, ***STABLE*** from 60 to 585min and ***SEVERE*** from 60 to 585min. The conclusions were obtained as follows:

1) At ***INITIAL***, the main wear mechanisms of peeling and plough were obtained. TiAl-10wt.%Ag was repeatedly squeezed at the effect of high pressure stress, resulting in the strengthening of work hardening, and the improving of subsurface hardness of wear scar, as well as the gradual lowering of friction coefficient and wear rate.

2) At ***FAST***, the primary wear mechanism was abrasive wear. Solid lubricant Ag showed the upward tendency for its plastic deformation, and wear debris exhibited the downward trend, leading to the forming of mixed layer containing massive Ag, and the gradual lowering of friction coefficient and wear rate.

3) At ***STABLE***, under the condition of the wear mechanism of plastic deformation, the lubricant film of antifriction and antiwear behavior was formed for the plastic

deformation of soft metal Ag. The excellent surface texture of Sa (0.398), Sq (0.359) and Sku (6.866) was obtained. The contact area between TiAl-10wt.%Ag and Si_3N_4 balls was improved, and the frictional resistance was decreased during the sliding wear, leading to the lowering of the subsurface hardness of wear scar, and the improving of the tribological behavior of TiAl-10wt.%Ag.

4) At ***SEVERE***, the main wear mechanisms were severe peeling and abrasive wear. The lubricant film of excellent lubricating property was gradually destroyed for the propagation of fatigue crack. The poor surface texture of Sa (0.486), Sq (0.445) and Sku (7.865) was obtained. The contact area between TiAl-10wt.%Ag and Si_3N_4 balls was lowered, and the frictional resistance was improved during the sliding wear, resulting in the improving of the subsurface hardness of wear scar, and the lowering of the tribological behavior of TiAl-10wt.%Ag.

5) The excellent tribological behavior at ***STABLE*** was obtained for the existence of lubricant film of excellent lubricating property, if compared to those at ***INITIAL***, ***FAST*** and ***SEVERE***.

6) The period of stable wear of TiAl-10wt.%Ag was significantly prolonged for the lubricant film of antifriction and antiwear behavior, if compared to that of TiAl alloy.

7) TiAl-10wt.%Ag for its excellent tribological behavior could be chosen as the promising structure material of mechanical components in the industries of aerospace and automotive.

Acknowledgments

This work was supported by the National Natural Science Foundation of China

(51275370); Self-determined and Innovative Research Funds of WUT (135204008); Fundamental Research Funds for the Central Universities (2015-yb-008 and 2015-zy-051); Authors also wish to gratefully thank the Material Research and Testing Center of Wuhan University of Technology for their assistance.

References

1 S.Y. Sung, Y.J. Kim, Intermetallics, 2007, **15**, 468.

2 X.H. Wu, Intermetallics, 2006, **14**, 1114.

3 C.M. Austin, Curr. Opin. Solid State Mater. Sci, 1999, **4**, 239.

4 F.H. Fores, C. Suryanarayana, D. Eliezer, J Mater Sci, 1992, 27, 5113.

5 T. Kawabata, H. Fukai, O. Izumi, Acta Materialia, 1998, **46**, 2185.

6 A. Rastkar, A. Bloyce, T. Bell, Wear, 2000, **240**, 19.

7 C. Li, J. Xia, H. Dong, Wear, 2006, **261**, 693.

8 K. Miyoshi, B. Lerch, S. Draper, Tribol Int, 2003, **36**, 145.

9 T. Sun, Q.D. Wang, L. Sun, G.H. Wu, Y. Na, Wear, 2010, **268**, 693.

10 W.Z. Zhai, X.L. Shi, M. Wang, Z.S. Xu, Tribol. Trans., 2014, **57(3)**, 416.

11 Z.S. Xu, L. Chen, Tribol. Trans., 2015, DOI:10.1080/10402004.2014.1002596.

12 D.W. Dareing, S. Atluri, Tribol. Trans., 1997, **40(3)**, 413.

13 Y.T. Peng, Z.Q. Wang, RSC Adv., 2014, **4**, 9980.

14 Y. Zhang, H. Tang, X.R. Ji, C.S Li, L. Chen, D. Zhang, RSC Adv., 2013, **3**, 26086.

15 K. Yang, X.L Shi, W.Z. Zhai, L. Chen, Q.X. Zhang, RSC Adv., 2015, **5**, 44618.

16 Y. Ming, X. Chen, V.P. Lin, Y.W. Dravid, Tribol. Trans., 1993, **36(3)**, 491.

17 Z.S. Xu, X.L. Shi, Q.X. Zhang, W.Z. Zhai, Tribol. Trans., 2014, **57(6)**, 1017.

18 Z.S. Xu, B. Xue, X.L. Shi, Q.X. Zhang, Tribol. Trans., 2015, **58**, 87.

19 I. Ahmad, Kennedy., Y.Q. Zhu, Wear, 2010, **269**, 71.

20 X.L. Shi, Z.S. Xu, M. Wang, W.Z. Zhai, J. Yao, Wear, 2013, **303(1-2)**, 486.

21 Y.M. Xu, H.F. Zuo, M. Zheng, JCIS., 2013, **9(11)**, 4239.

22 ASTM E92-82, Standard test method for vickers hardness of metallic materials, ASTM International, 2003.

23 ASTM B962-08, Standard test methods for density of compacted or sintered powder metallurgy (PM) products using Archimedes' principle, ASTM International, 2008.

24 ASTM G99-95, Standard test method for wear testing with a pin-on-disk apparatus, ASTM International, 1995.

25 R.D. Tyagi, S. Xiong, J.L. Li, Wear, 2011, **270**, 423.

26 G. Evan, B.J. Hockey, R.W. Rice, II. US Govt. Printing Office, 1979, 1.

27 C. Rynio, H. Hattendorf, J. Klöwer, G. Eggeler, Wear, 2014, **315**, 1.